Evidence of a Purely Electronic Two-Dimensional Lattice at the Interface of TMD/Bi_2Se_3 Heterostructures

Zachariah Hennighausen,[1] Christopher Lane[1], Ioana Gianina Buda[1], Vineet K. Mathur[1], Arun Bansil[1], and Swastik Kar[1,*]
[1]Department of Physics, Northeastern University, Boston, MA 02115

Supporting Information

1. Diophantine equation and guidance on mathematically calculating the electronic moiré lattice commensurate unit cell.

2. Demonstration that the experimentally observed moiré spots are not due to one of the parent crystals.

3. Data demonstrating that the electronic moiré lattice was observed in other 2D heterostructures

4. Explanations for why wave-interference and double diffraction are very unlikely to induce the moiré superlattice spots in high-energy (200keV) SAED

5. Discussion of previous work on using different types of experimental and theoretical electron diffraction to study moiré patterns and charge redistribution

6. Optical measurements indicating that the parent layers are well-coupled, and a moiré superlattice is forming

1. Diophantine equation and guidance on mathematically calculating the electronic moiré lattice commensurate unit cell.

The below equations were used to mathematically calculate the moiré superlattice commensurate unit cell parameters, where m, n, r, and s are the unit cell parameters.[1,2] For the equations to be satisfied, all the lattice parameters must be integers. Eq.1 is Diophantine and used to calculate the moiré superlattice commensurate unit cell length. Eq.2 was used in Figure SI.1. Eq.3 is used to calculate the relative rotation of the moiré superlattice relative to the Bi_2Se_3 crystal. Eq.1 and Eq.3 were used to calculate the parameters shown in Figure 2d and Section 3.

$$Length_{moiré} = a_{Bi_2Se_3}\sqrt{m^2 + n^2 - mn} = a_{TMD}\sqrt{r^2 + s^2 - rs} \quad \text{Eq.1}$$

$$lattice\ ratio = \frac{a_{Bi_2Se_3}}{a_{TMD}} \quad \text{Eq.2}$$

$$\cos\left(\varphi_{moiré,Bi2Se3}\right) = \frac{m-\frac{n}{2}}{\sqrt{m^2+n^2-mn}} \quad \text{Eq.3}$$

Next we will discuss the mathematics of how a moiré pattern is formed because it provides insight into the interlayer coupling. Moiré patterns only develop when two lattices interact through an effective multiplication - simply summing two lattices does not produce a moiré pattern.[1–4] The Fourier transform is a linear operation: $\mathcal{F}[af(x) + bg(x)] = a\mathcal{F}[f(x)] + b\mathcal{F}[g(x)]$, where $f(x)$ and $g(x)$ are functions. Summing two functions does not produce any new frequencies. However, when two non-identical functions are multiplied, they will produce a new frequency: $\mathcal{F}[af(x) \cdot bg(x)] = abF[f(x)] * F[g(x)] \neq aF[f(x)] + bF[g(x)]$, where $*$ is the convolution operation. This new frequency is the moiré pattern. The presence of moiré superlattice spots when using SAED indicates that the two materials are being "multiplied", a process facilitated through the interlayer coupling.

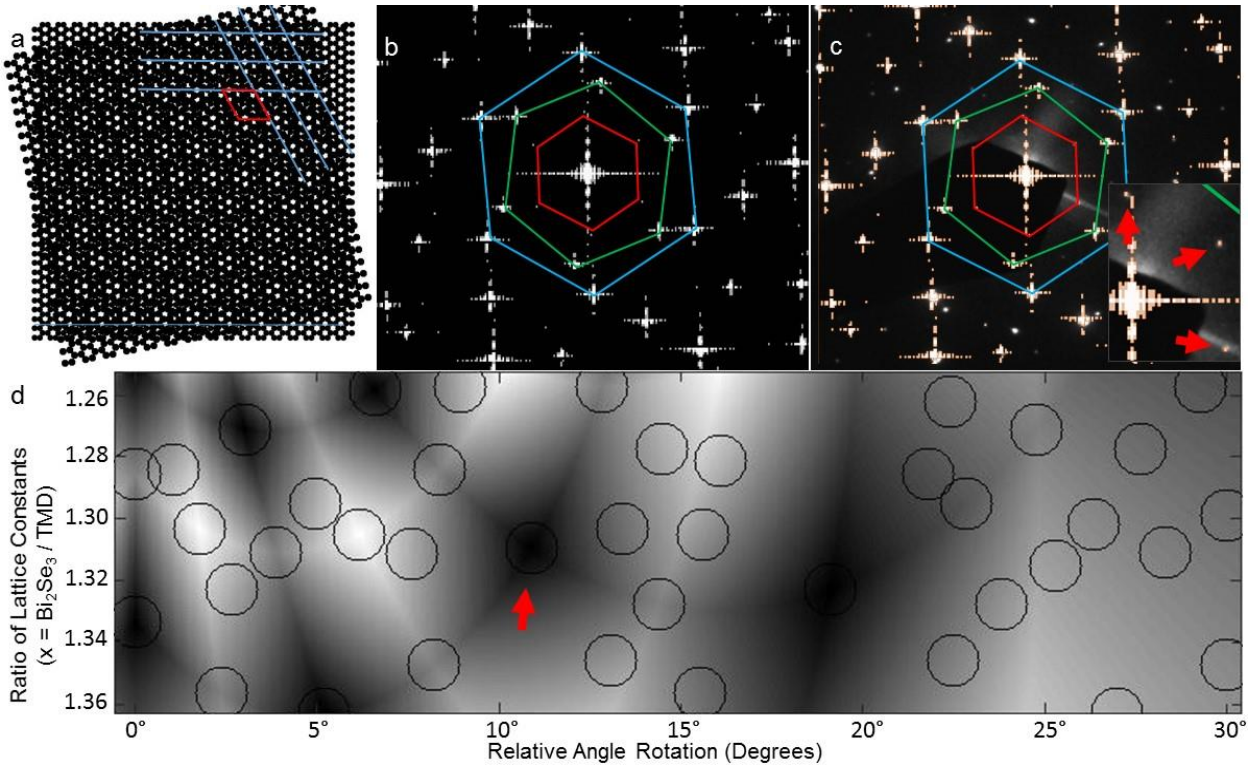

Figure S1. Guidance on calculating the moiré superlattice commensurate unit cell. (a) Matlab generated model of the 2D heterostructure in Figure 1e. (b) Fourier transform of the model in (a). (c) The Fourier transform was shaded orange and then overlaid on the experimental SAED data shown in Figure 1e (white spots). The near perfect alignment indicates that the model sufficiently captures the system. (d) Plot showing 2D heterostructure configurations that produce smaller (m, n, r, and s are all less than 10) moiré superlattice commensurate unit cells, using the relative rotation (or twist angle) and ratio of lattice constants (Eq.2) are input parameters.[1,2] The intersection of dark or light lines indicate regions where a commensurate unit cell is more like to found. See the corresponding references for more thorough guidance on interpreting the graph.[1,2] The red arrow highlights the location that corresponds to the 2D heterostructure in (a), (b), and (c), indicating that the moiré superlattice parameters have been identified.

2. Demonstration that the experimentally observed moiré spots are not due to one of the parent crystals.

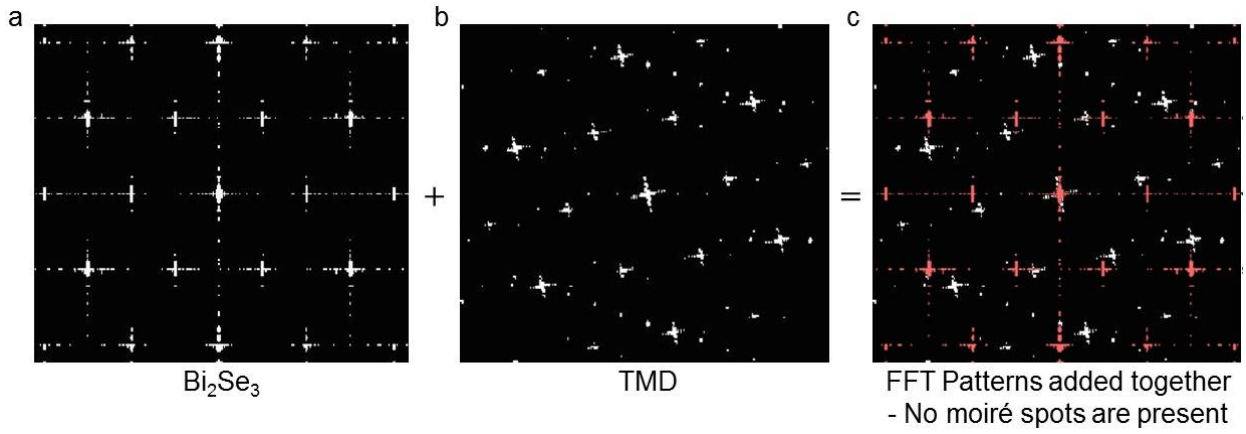

Figure S2. The moiré SAED spots are not a product of one of the individual lattices. (a) The Fourier transform of a model of a Bi_2Se_3 lattice, and (b) and the Fourier transform of a representative monolayer TMD lattice. (c) TMD transform was colored in red and overlaid on the Bi_2Se_3 transform. None of the images contain the moiré superlattice spots, demonstrating that an effective multiplication and interaction of the lattices is needed to produce them (see Figure S1 for more information).

3. **Data demonstrating that the electronic moiré lattice was observed in other 2D heterostructures**

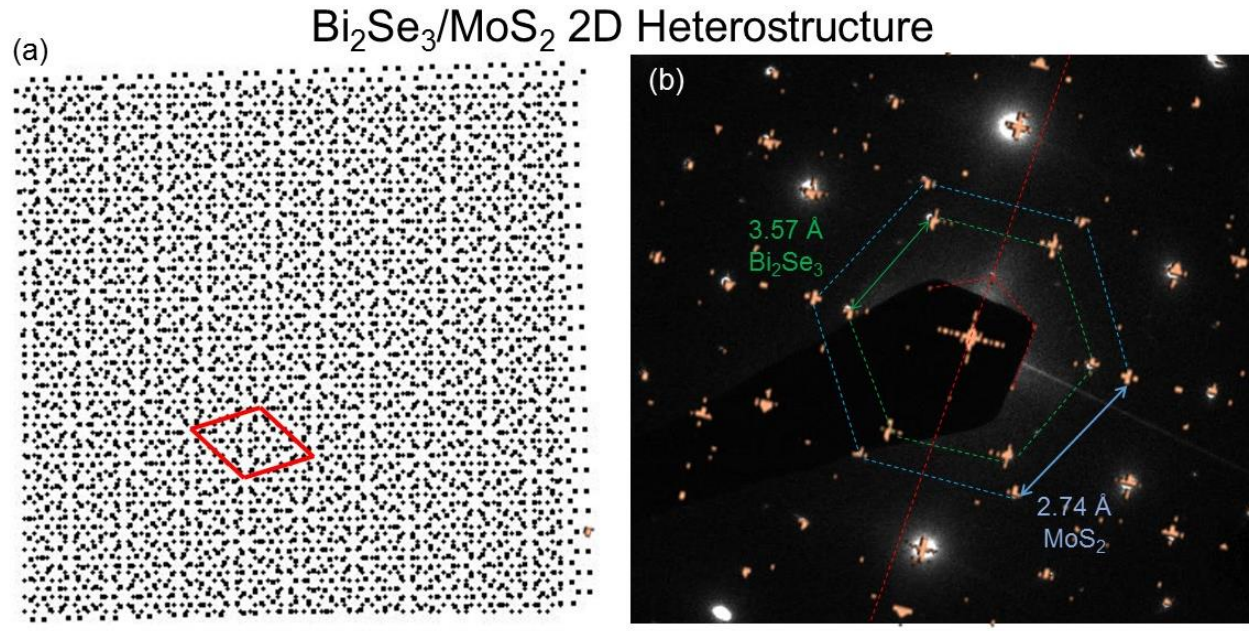

(c)	Lattice ratio	Moiré lattice length	Angle: MoS_2 to Bi_2Se_3	Angle: Moiré to Bi_2Se_3	m	n	r	s
Commensurate unit cell	1.303	2.741nm	1.772°	7.59°	7	1	9	1
Modeling	1.302	1.37nm/2.74nm	1.7°	7.6°				
Experiment	1.30±0.02	1.37nm±0.021	1.7°±0.2°	7.7°±0.3°				

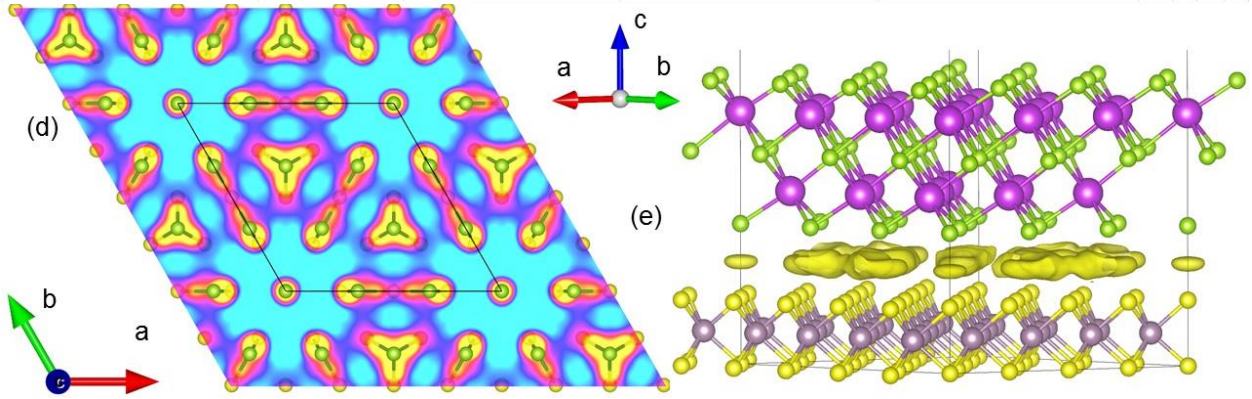

Figure S3. Experimental, moiré modeling, and DFT data for a Bi_2Se_3/MoS_2 2D heterostructure. The data suggests high energy electrons are diffracting off interlayer coupling induced scattering sites, which DFT predicts to be located between nearest interlayer neighbors. (a) Real-space model of the 2D heterostructure in (b) using the techniques described in Section S1. (b) High-voltage (200keV) SAED experimental data with the Fourier transformed model from (a) overlaid on top. The strong overlap of the spots suggests the model and experiment are in agreement, and that the model captures the system sufficiently. (c) Table with the data summarized, demonstrating that theory and experiment are in very good agreement. (d) DFT calculated interlayer charge distribution in the interlayer region between both layers. (e) Cross-section view of a DFT calculated 2D heterostructure with the interlayer coupling induced charge pools shown. The DFT calculated 2D heterostructure is different from the parameters in (d) due to computational limitations; however, the calculated structure is very similar where the twist angle was made 0°, vice 1.7°, making the lattice parameters (3, 0, 4, 0 for m, n, r, and s, respectively).

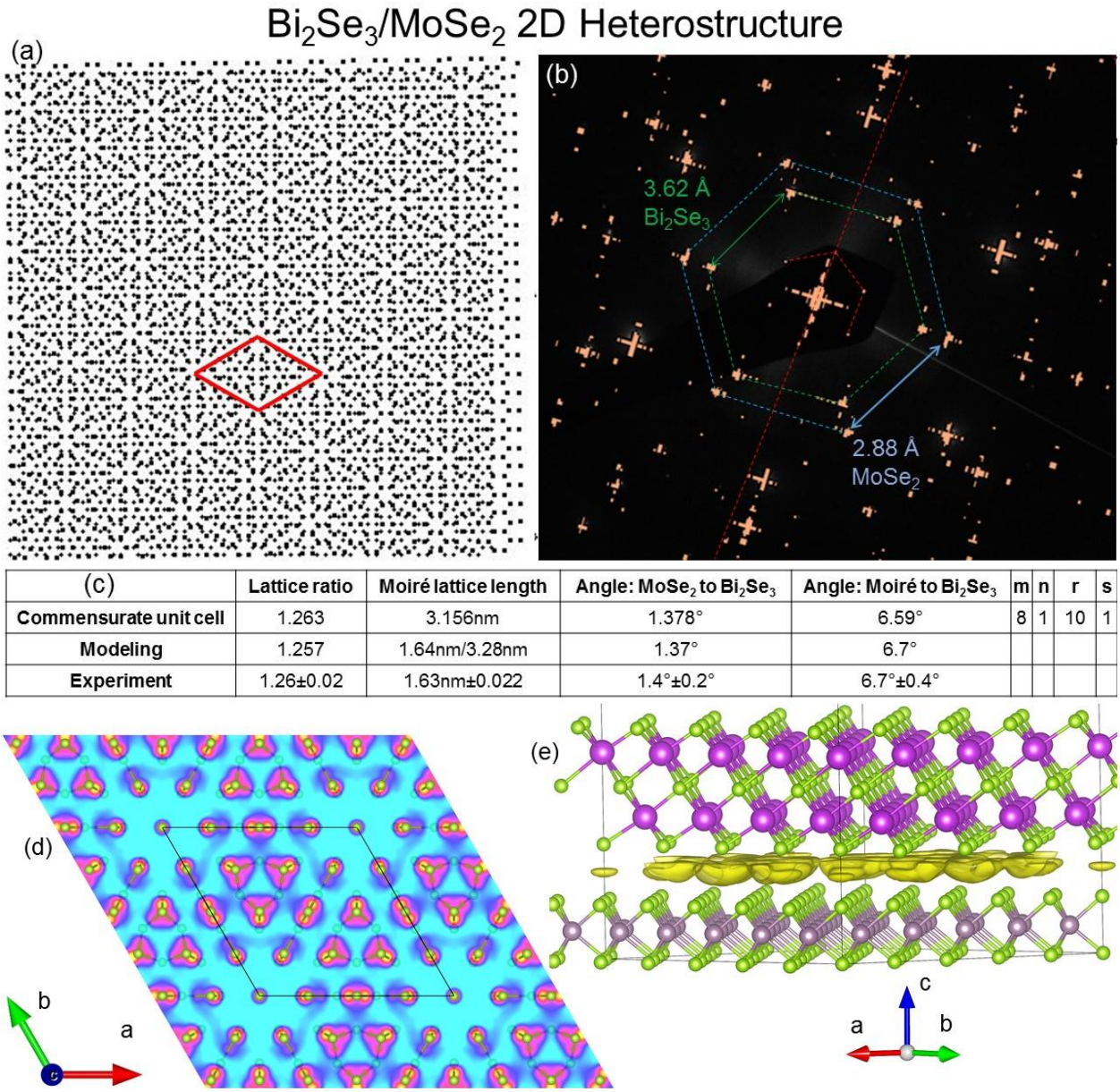

(c)	Lattice ratio	Moiré lattice length	Angle: $MoSe_2$ to Bi_2Se_3	Angle: Moiré to Bi_2Se_3	m	n	r	s
Commensurate unit cell	1.263	3.156nm	1.378°	6.59°	8	1	10	1
Modeling	1.257	1.64nm/3.28nm	1.37°	6.7°				
Experiment	1.26±0.02	1.63nm±0.022	1.4°±0.2°	6.7°±0.4°				

Figure S4. Experimental, moiré modeling, and DFT data for a $Bi_2Se_3/MoSe_2$ 2D heterostructure. Taken together, the data suggests high-voltage electrons are diffracting off interlayer coupling induced scattering sites, which DFT predicts to be located between nearest interlayer neighbors. (a) Real-space model of the 2D heterostructure in (b) using the techniques described in Figure SI.1. (b) High-voltage (200keV) SAED experimental data with the Fourier transformed model from (a) overlaid on top. The strong overlap of the spots suggests the model and experiment are in agreement, and that the model captures the system sufficiently. (c) Table with the data summarized, demonstrating that theory and experiment are in very good agreement. (d) DFT calculated interlayer charge distribution in the interlayer region between both layers. (e) Cross-section view of a DFT calculated 2D heterostructure with the interlayer coupling induced charge pools shown. The DFT calculated 2D heterostructure is different from the parameters in (d) due to computational limitations; however, the calculated structure is very similar where the twist angle was made 0°, vice 1.7°, making the lattice parameters (4, 0, 5, 0 for m, n, r, and s, respectively).

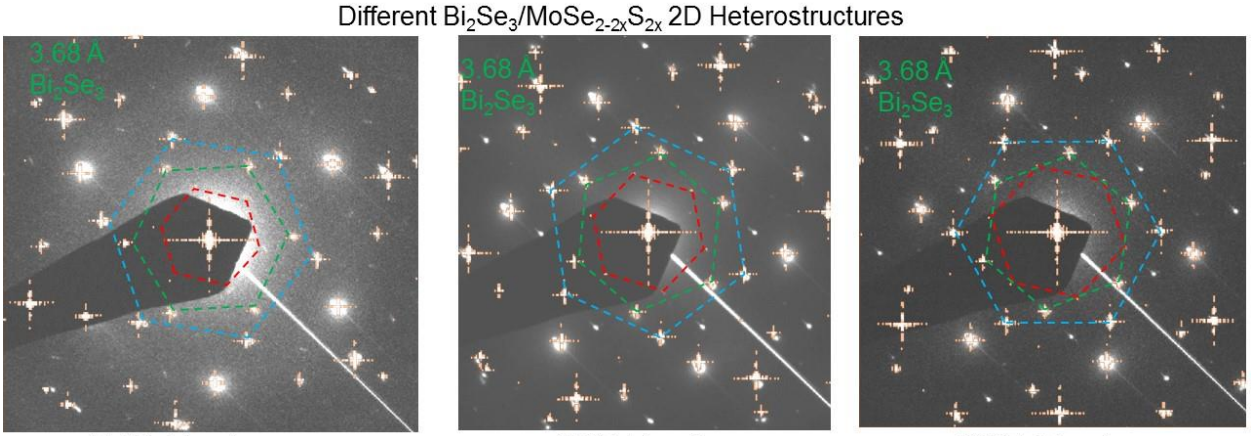

Experimental Data	Lattice Ratio	Angle
$MoSe_{2-2x}S_{2x}$/ Bi_2Se_3	1.301	12.5°
Bi_2Se_3/ Moiré lattice	1.51	16.8°

Experimental Data	Lattice Ratio	Angle
$MoSe_{2-2x}S_{2x}$/ Bi_2Se_3	1.302	15.3°
Bi_2Se_3/ Moiré lattice	1.34	24.7°

Experimental Data	Lattice Ratio	Angle
$MoSe_{2-2x}S_{2x}$/ Bi_2Se_3	1.295	20.6°
Bi_2Se_3/ Moiré lattice	1.15	24.8°

Moiré superlattices calculated using Diophantine equations

Lattice ratio	Moiré lattice length	Twist Angle: $MoSe_{2-2x}S_{2x}$ to Bi_2Se_3	Angle: Moiré to Bi_2Se_3	m	n	r	s
1.298	3.715nm	12.69°	17.0°	10	3	12	1
1.305	2.543nm	15.61°	25.3°	7	3	9	6
1.296	4.364nm	20.83°	24.5°	12	5	14	1

Figure S5. Experimental and moiré modeling images for different $Bi_2Se_3/MoSe_{2-2x}S_{2x}$ 2D heterostructures at various twist angles. The data demonstrates that the method can not only be applied to arbitrary twist angles, but can also be used on alloy-based 2D structures. Despite the fact that the sulfur and selenium atoms appear to be randomly distributed, the monolayer TMD still forms a crystal, and this crystal is able to form a significant interlayer coupling with the Bi_2Se_3. Interestingly, the Bi_2Se_3 appeared to grow with slightly different lattice constants across different monolayer TMDs, but kept the same lattice constant when growing on $MoSe_{2-2x}S_{2x}$, despite the fact that the $MoSe_{2-2x}S_{2x}$ lattice constant fluctuated. The fluctuation in $MoSe_{2-2x}S_{2x}$ is believed to be due to the changing sulfur and selenium concentrations. Photoluminescence values were always between signature monolayer MoS_2 and $MoSe_2$ values, but varied across samples, suggesting different crystals contained different ratios of sulfur to selenium, which offers an explanation why the monolayer $MoSe_{2-2x}S_{2x}$ lattice constant fluctuated.

DFT calculations on the alloy 2D heterostructures were not completed due to computational limitations. To the best of our knowledge, the sulfur and selenium atoms are randomly distributed, therefore requiring very large supercells that are able to properly capture the random placement. Due to the massive size of the moiré superlattices, we could not confirm whether the Diophantine equation matches exactly; however, to the best of our knowledge, the Diophantine predictions above in the second table are accurate.

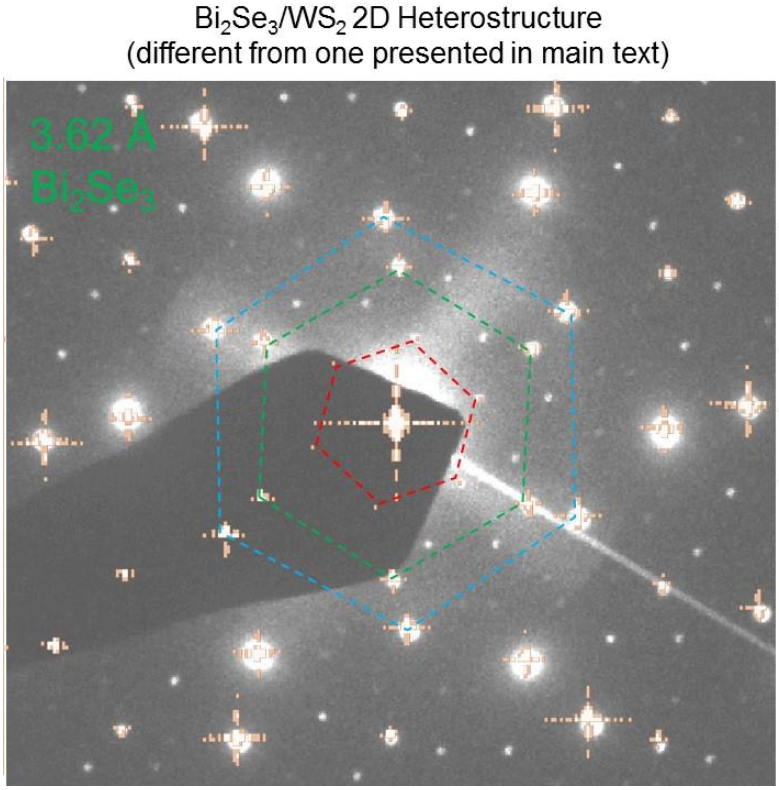

4.71° twist angle

Experimental Data	Lattice Ratio	Angle
WS_2/ Bi_2Se_3	1.312	4.71°
Bi_2Se_3/ Moiré lattice	1.77	11.9°

Modeling Data	Lattice Ratio	Angle
WS_2/ Bi_2Se_3	1.312	4.71°
Bi_2Se_3/ Moiré lattice	1.77	12.0°

Figure S6. Experimental and moiré modeling images for a Bi_2Se_3/WS_2 2D heterostructure (with a different twist angle from that in the main text). The image is presented on its own to better show the moiré superlattice spots, and the strong agreement between the model and the experimental data.

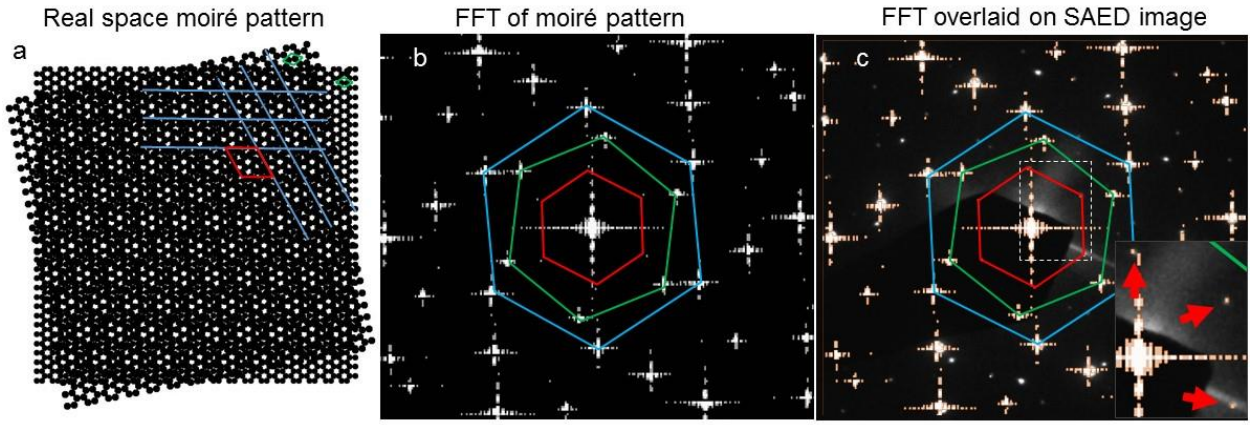

d

	Lattice ratio	Moiré lattice length	Angle: WS_2 to Bi_2Se_3	Angle: Moiré to Bi_2Se_3	m	n	r	s
Commensurate unit cell	1.309	1.106nm	10.89°	19.1°	3	1	4	2
Modeling	1.31	1.11nm	10.9°	19.1°	3	1	4	2
Experiment	1.31±0.02	1.11nm±0.012	10.9°±0.2°	19.1°±0.2°				

Figure S7. Experimental and moiré modeling images for Bi_2Se_3/WS_2 2D heterostructures from Figure 2. A complete explanation can be found in Figure 2. The information lattice information from solving the Diophantine equation is included in this figure (i.e., the m, n, r, and s data).

4. Explanations for why wave-interference or double diffraction are very unlikely to induce the moiré superlattice spots in high-energy (200keV) SAED

Here we aim to address the question: Why is the observed moiré pattern (or new lattice) not simply due to wave-interference? We have split the explanation into two parts. PART I – Three different wave-interferences are described, along with explanations rebutting them for high-energy SAED of 2D materials. PART II – A representative HR-TEM imaging and high-energy SAED measurements of a bilayer MoS_2 2D structure, where a moiré pattern is clearly observed using HR-TEM, but is noticeably absent in the SAED measurement. The fact that moiré superlattice spots cannot be detected suggests wave-interference is not present in high-energy SAED of 2D materials.

PART I

Figure 2 of the main manuscript shows simplified descriptions of pertinent SAED concepts that are helpful to understand the below explanations. Although interference occurs when waves interact, a moiré pattern is only produced when the conditions are correct. Three different interference mechanisms are described below, which have been observed in optical systems, but are very unlikely in our 2D heterostructures.

FIRST – Superposition of diffracted wave fronts

As shown in Figure 2, there are only discrete directions along which the Bragg condition is satisfied (i.e., the sum of electron amplitudes is non-zero), and all remaining directions are zero. The moiré spots are physically located at a portion of the screen where the TMD and Bi_2Se_3 diffraction values are zero. Since there is no way a new "non-zero-amplitude" direction can be created by interference of the two lattice layers (i.e., two zeros cannot produce a non-zero amplitude), it stands to reason that the third set of spots necessarily arises from a third lattice layer.

SECOND – Strong reflections in upper lattice become initial waves for lower lattice (i.e. double diffraction)

Our systems consist of a periodic array of scatters overlaid on a second array of scatters. In such systems, if the upper lattice projects a diffraction pattern onto the lower lattice, the two lattices are effectively multiplied, thereby producing a moiré pattern. This concept is shown in Figure S8 using an optical setup.[1]

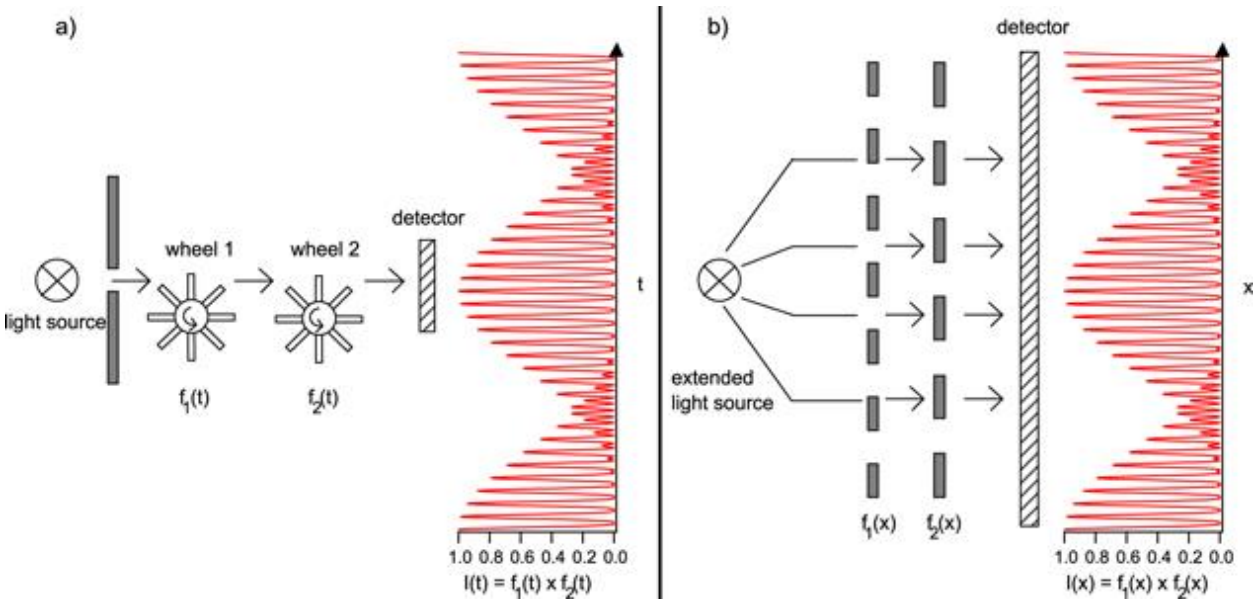

Figure S8. Formation of 1-dimensional moiré patterns using two different optical setups. (a) Moiré pattern in time space $I(t)$: two consecutive identical rotating wheels with evenly spaced blockers are located between the coherent light source and detector. (b) Moiré pattern in real space $I(x)$: plane waves of coherent light are incident onto two consecutive lattices. To form the moiré pattern, lattice $f_1(x)$ projects a diffraction pattern onto lattice $f_2(x)$. This figure and portions of the caption are reprinted with permission (CC BY).[1]

In sharp contrast to optical systems, such a scenario is mathematically very unlikely using SAED of 2D heterostructures. In high-energy SAED, electrons elastically scatter at low angles (0.6°), while photons frequently scatter more than 70°. The low scattering angles, combined with the atomically thin nature, suggest that the first electrons do not begin to interact with each other until traveling more than 26 nm in the vertical direction (after being scattered). Additionally, they likely do not form proper diffraction patterns until they have traveled more than 100nm in the vertical direction. This is supported by the below geometric equations, which assume monolayer MoS_2 is the upper lattice. This is a conservative assumption since the lattice

spacing is smaller than Bi_2Se_3, $MoSe_2$, and WS_2. *N* - Number of Atomic Spacings - is the number of upper-most sulfur atoms (i.e., the top most layer of monolayer MoS_2) in one moiré superlattice unit cell, that are also spaced along the same diffraction line. *S* – Upperlattice spacing – is the distance between the diffraction planes. Θ – scattering angle – is defined in Figure S9. d – vertical distance – is the vertical distance traveled by the electron after initial scattering.

$$N * {}^{S}/_{\tan(\theta)} = d$$

$$4 * {}^{0.28\ nm}/_{\tan(0.6°)} = 107\ nm$$

With this said, if the sample being measured is bulk (e.g., greater than approximately 100nm thick), then double diffraction is conceivable, and has been previously observed.[5] Despite this, to the best of our knowledge, it has never been demonstrated in 2D materials. In fact, the only other known publication to demonstrate high-energy (80keV) SAED moiré diffraction spots of a 2D material, disqualified double diffraction using similar logic.[6]

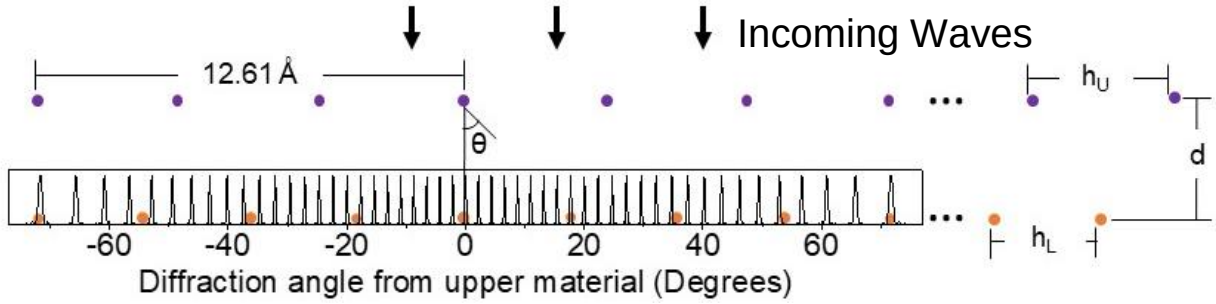

Figure S9: Simplified diagram of a possible double diffraction scenario. Strong reflections in upper lattice become initial waves for lower lattice, often resulting in the upper lattice projecting a diffraction pattern onto the lower lattice. The calculation for the diffraction pattern shown above is not realistic, but was created for demonstration. Each scattering site is assumed to scatter evenly from 0° to 90°, whereas in SAED the scattering profile is non-linear and is concentrated around lower angles. As such, the angle profile is not realistic for SAED, since it extends to 60° on either side, and SAED scatters are angles of ~0.6°

THIRD – Long wavelength interacts with both lattices simultaneously

This form of interference is able to occur when the wavelength is long enough to interact with both lattices at the same time (i.e., the interlayer distance between the lattice's is less than half a

wavelength). Although this effect has been previously demonstrated for bilayer graphene 2D structures using very low-energy electrons (~200eV),[7] it is very unlikely to be the case here because the interlayer separation is ~40x that of the electron wavelength.

In summary, wave-interference - described using the three explanations above - is very unlikely to produce the new lattice spots observed in our 2D heterostructures, lending support for our explanation that an electronic lattice residing in the interlayer region is diffracting electrons.

PART II

Below are representative SAED measurements from two different TMD-based 2D structures where moiré superlattice spots cannot be detected, suggesting wave-interference is not present in high-energy SAED.

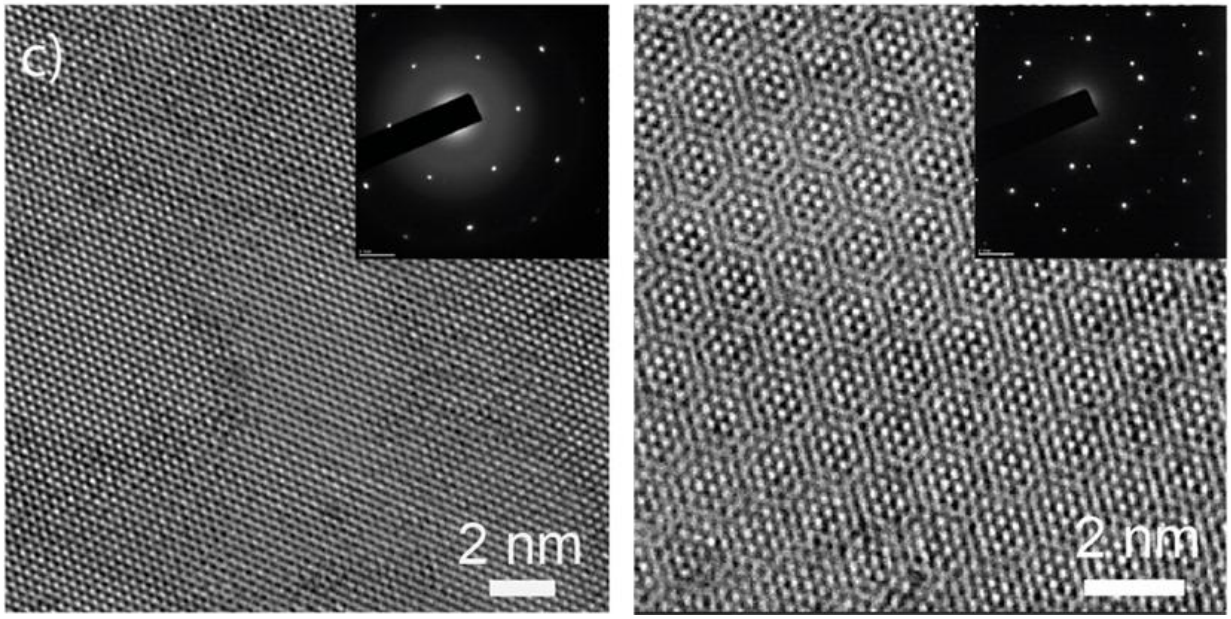

Figure S10. Suspended monolayer MoS_2 and bilayer MoS_2-MoS_2 samples. High-resolution TEM images of a typical MoS_2 monolayer (left side) and a bilayer MoS_2 (right side) sample with corresponding SAED images as insets. Despite the fact that HR-TEM imaging of bilayer MoS_2 clearly shows a moiré pattern, SAED shows no such indications, suggesting wave-interference of the layers is not present in SAED, but that a unique electronic lattice is present. This figure has been reprinted with permission.[8]

5. Discussion of previous work on using electron diffraction to study moiré patterns and interlayer bonding

SAED is a powerful tool used to observe the reciprocal space of samples. If a periodic arrangement of scattering sites with a sufficient high cross exists (e.g., a lattice), spots will appear.[9] Spots closer to the center correspond to crystals with a larger periodicity, which is why the monolayer TMD has the largest radius and the electronic moiré lattice has the smallest. Other electron diffraction methods (e.g., CBED) have been used to reveal bonding,[10] and low energy electrons (~236eV) have revealed the moiré pattern in bilayer graphene structures; however, both these situations involve different physics and scattering mechanisms. CBED functions with different assumptions, and is able to reveal significantly more information.

2D Structure moiré patterns have been previously shown using TEM imaging; however, the electron-material interaction mechanisms between imaging and SAED are different, allowing each method to provide unique information. TEM imaging is a different process involving both inelastic and elastic scattering, as well as charge induced phase shifts. SAED, on the other hand, only detects electrons elastically scattered at low angles (~0.6°), where bright spots are the product of periodically spaced scattering sites.[9] Observation of periodic bright spots in SAED is strong evidence that a "lattice" of scattering sites exists. Further, the scattering cross section is dependent on not only the total charge, but also the shape,[9] suggesting the scattering sites have well-formed shapes (i.e., the charge redistribution was not diffusive). These conclusions are in agreement with previously published synchrotron X-ray diffraction experiments, which showed charge accumulation between the layers of bulk TiS_2, suggesting the "weak" van de Waals bonding induces sufficient charge redistribution that leads to the formation of a polar bond.[11]

The observation of SAED spots using high energy electrons, suggests the electronic moiré lattice has a relatively large scattering cross section. It has been previously shown that, when used in conjunction with DFT, scattering data is able to measure the magnitude and shape of charge redistribution.[10,11] Although performing such a robust analysis is beyond the scope of this paper, we are able to infer a relative range of scattering cross section values by comparing the relative brightness (i.e., photon counts) of the SAED spots. The electronic moiré lattice SAED spots are 1-6% the intensity of the monolayer TMD spots, suggesting an approximate range of values that

would be very large for non-atomic scattering sites. The scattering cross section is determined not only by the magnitude of charge, but also by the distribution,[5,9] where well-formed sites are more likely to scatter than very diffuse clouds. Bloch-wave simulations could provide further insight into the presence of a possible 2D electronic lattice; however, such simulations are computationally expensive and difficult, and are beyond the scope of this work.

6. Optical measurements indicating the parent layers are well-coupled, and a moiré superlattice is forming

The below data suggests that a strong interlayer coupling exists within Bi_2Se_3/TMD 2D heterostructures, which induces the formation of a moiré superlattice and a unique bandstructure. This is in agreement with a principle claim of this work that the interlayer coupling is sufficiently strong to induce significant charge redistribution into the interlayer region.

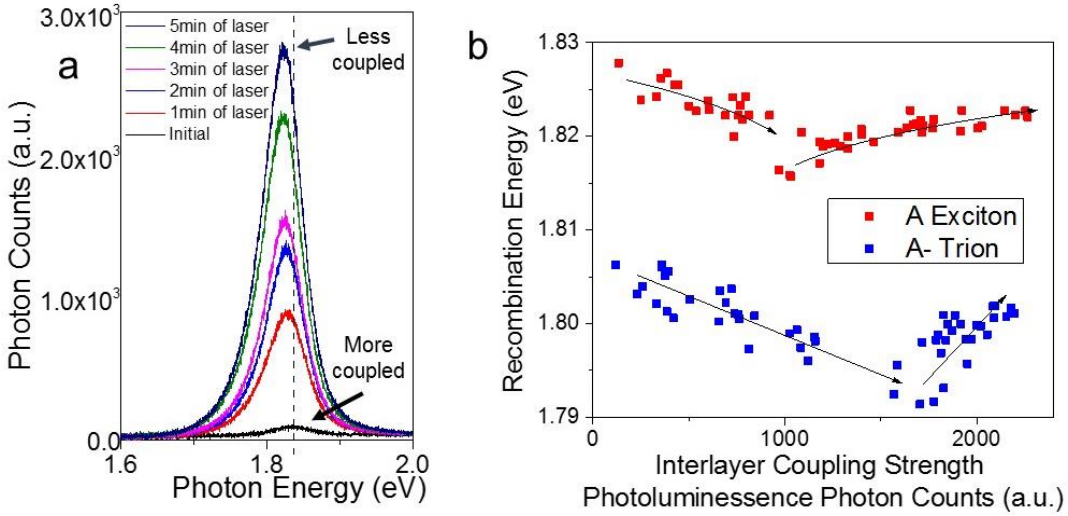

Figure S11. Changes in exciton binding energy as a function of interlayer coupling strength. (a) Previous work demonstrated that the interlayer coupling can be modified using laser-exposure in an oxygen-present atmosphere, where the coupling strength is dependent on the amount of exposure and partial pressure of oxygen.[12] The PL spectra can be decomposed into its excitonic and Lorentzian contributions.[13] (c) Changes to the recombination energy as a function of interlayer coupling suggests an influential interlayer coupling exists that is forming a moiré superlattice. The interlayer coupling strength is inferred using the PL intensity. (a) is reprinted with permission.[12]

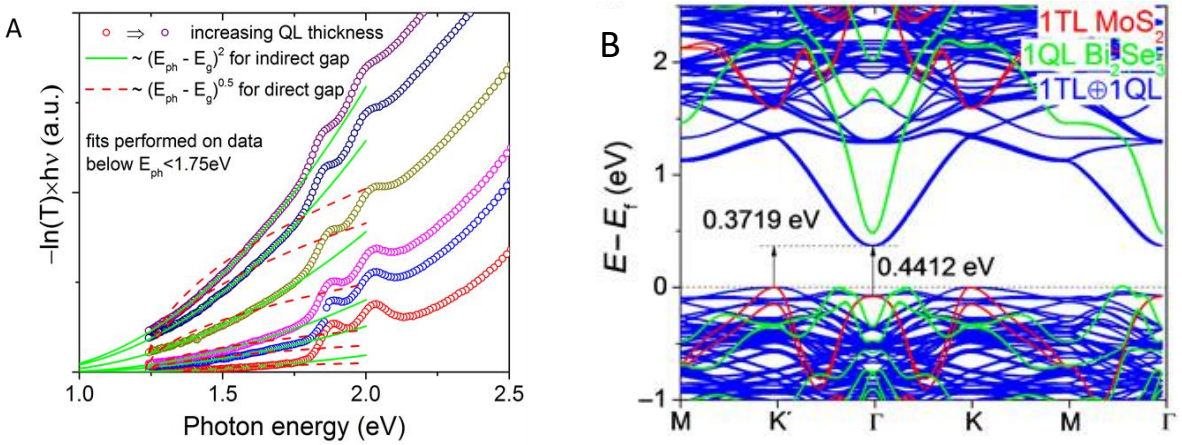

Figure S12. DFT DoS calculations and Tauc plots from experimentally measured absorption data. (A) Tauc plot fits using both η=2 (red dashed lines) and η=1/2 (green solid lines) of Bi_2Se_3/MoS_2 2D heterostructures, suggesting that these are indeed indirect band gap systems. (B) DFT-calculated band structure of a Bi_2Se_3/MoS_2 2D heterostructure,

where the results predict the interlayer coupling induces the formation of a new, unique bandstructure, distinct from either parent crystal. The results suggest that the as-grown Bi_2Se_3/TMD 2D heterostructures contain a new band structure that corresponds to the moiré superlattice. This data is reprinted with permission (CC BY-NC 4.0).[14]

References

1. Zeller, P. & Günther, S. What are the possible moiré patterns of graphene on hexagonally packed surfaces? Universal solution for hexagonal coincidence lattices, derived by a geometric construction. *New J. Phys.* **16**, 083028 (2014).
2. Zeller, P., Ma, X. & Günther, S. Indexing moiré patterns of metal-supported graphene and related systems: strategies and pitfalls. *New J. Phys.* **19**, 013015 (2017).
3. Lebanon, G. & Bruckstein, A. M. On Designing Moiré Patterns. in *Visual Attention Mechanisms* (eds. Cantoni, V., Marinaro, M. & Petrosino, A.) 205–217 (Springer US, 2002). doi:10.1007/978-1-4615-0111-4_19
4. Lebanon, G. & Bruckstein, A. M. Variational approach to moiré pattern synthesis. *JOSA A* **18**, 1371–1382 (2001).
5. Thomas, J. & Gemming, T. *Analytical Transmission Electron Microscopy: An Introduction for Operators*. (Springer Netherlands, 2014).
6. Yoo, H. *et al.* Atomic and electronic reconstruction at the van der Waals interface in twisted bilayer graphene. *Nat. Mater.* 1 (2019). doi:10.1038/s41563-019-0346-z
7. Latychevskaia, T., Escher, C. & Fink, H.-W. Moiré structures in twisted bilayer graphene studied by transmission electron microscopy. *Ultramicroscopy* **197**, 46–52 (2019).
8. Waduge, P. *et al.* Direct and Scalable Deposition of Atomically Thin Low-Noise MoS2 Membranes on Apertures. *ACS Nano* **9**, 7352–7359 (2015).
9. Bendersky, L. A. & Gayle, F. W. Electron Diffraction Using Transmission Electron Microscopy. *J. Res. Natl. Inst. Stand. Technol.* **106**, 997–1012 (2001).
10. Nakashima, P. N. H., Smith, A. E., Etheridge, J. & Muddle, B. C. The Bonding Electron Density in Aluminum. *Science* **331**, 1583–1586 (2011).

11. Kasai, H. *et al.* X-ray electron density investigation of chemical bonding in van der Waals materials. *Nat. Mater.* **17**, 249 (2018).

12. Hennighausen, Z. *et al.* Oxygen-Induced In-Situ Manipulation of the Interlayer Coupling and Exciton Recombination in Bi2Se3/MoS2 2D Heterostructures. *ACS Appl. Mater. Interfaces* (2019). doi:10.1021/acsami.9b02929

13. Mak, K. F. *et al.* Tightly bound trions in monolayer MoS_2. *Nat. Mater.* **12**, 207–211 (2013).

14. Vargas, A. *et al.* Tunable and laser-reconfigurable 2D heterocrystals obtained by epitaxial stacking of crystallographically incommensurate Bi2Se3 and MoS2 atomic layers. *Sci. Adv.* **3**, e1601741 (2017).